JOURNAL OF THE KOREAN ASTRONOMICAL SOCIETY
33: 1 ~ 17, 2000

SPH SIMULATIONS OF BARRED GALAXIES: DYNAMICAL EVOLUTION OF GASEOUS DISK

HONG BAE ANN[1] AND HYUNG MOK LEE[2]
[1]Department of Earth Sciences, Pusan National University, Pusan 609-735, Korea
[2]Astronomy Program, SEES, Seoul National University, Seoul 151-742, Korea
E-mail: hbann@cosmos.es.pusan.ac.kr, hmlee@astro.snu.ac.kr
(Received Apr. 7, 2000; Accepted Jun. 2, 2000)

ABSTRACT

We have performed extensive simulations of response of gaseous disk in barred galaxies using SPH method. The gravitational potential is assumed to be generated by disk, bulge, halo, and bar. The mass of gaseous disk in SPH simulation is assumed to be negligible compared to the stellar and dark mass component, and the gravitational potential generated by other components is fixed in time. The self-gravity of the gas is not considered in most simulations, but we have made a small set of simulations including the self-gravity of the gas. Non-circular component of velocity generated by the rotating, non-axisymmetric potential causes many interesting features. In most cases, there is a strong tendency of concentration of gas toward the central parts of the galaxy. The morphology of the gas becomes quite complex, but the general behavior can be understood in terms of simple linear approximations: the locations and number of Lindblad resonances play critical role in determining the general distribution of the gas. We present our results in the form of 'atlas' of artificial galaxies. We also make a brief comment on the observational implications of our calculations. Since the gaseous component show interesting features while the stellar component behaves more smoothly, high resolution mapping using molecular emission line for barred galaxies would be desirable.

Key words : galaxies : barred – galaxies : spirals – numerical simulations

I. INTRODUCTION

The fraction of barred galaxies among spirals is somewhat uncertain, but it tends to grow as more sensitive observations become available. Since the bar is a pattern of stellar material that rotates at a uniform angular speed, it provides fluctuating potential to stars and interstellar clouds that are differentially rotating according to the velocity curve generated by the galactic potential. The perturbed components could acquire significant non-circular velocity component after experiencing non-axisymmetric potential fluctuation. Many interesting phenomena develop as the clouds have significant random velocity components. The clouds can experience hydrodynamic collisions which tends to suppress the random velocity components. Thus, the kinematic behavior of the clouds should be significantly different from that of stars. Even for clouds, there could be some distinction between those experienced collisions and those without collisions.

There is a simple way to predict the dynamical structure of molecular clouds. In rotating frame of the bar, there are closed, non-intersecting orbits such as x1 and x2 families (Contopoulos & Mertzanides 1977; Contopoulos 1981). The fluctuating potential tends to generate non-circular orbits and the hydrodynamic collisions act as a 'filter' that allows only objects on closed orbits to survive. It has been customary to interpret the dynamical data of clouds using such orbit calculations (e.g., Binney et al. 1991). However, it is necessary to carry out self-consistent numerical calculations that takes into account hydrodynamic collisions. For example, Lee et al. (1999) have shown that the actual behavior of the gaseous disk is somewhat more complicated than simple minded analysis using orbit calculations. By comparing with the observed data, they concluded that the distribution of SPH particles closely resembles the dense interstellar clouds traced by molecular lines such as HCN and CS. The distribution of CO emission is less prominent than the high density tracers because the clouds with relatively low density may have had less collisions.

In the present study, we have performed a large number of simulations using SPH technique to investigate the response of the gaseous disk to the presence of a bar. We adopt simplified model for the gravitational potential of the galaxy, but vary the model parameters widely so that wide range of spiral galaxies can be mimicked. The response of the gas by the fluctuating potential is followed until the model galaxy reaches 'secular evolution' phase. It requires time scale of order of 10 rotations, and is around 10^9 years. Further evolution is governed by more complex processes such as stellar formation and evolution which cannot be easily incorporated in our simplified simulations. Thus the main purpose of the present study is to trace rather violent process that occurs just after the formation of the bar.

This paper is organized as follows. In next section,

we describe the numerical method very briefly. The model galaxy is discussed in Section III, and we present our results in Section IV. We discuss the implications of our simulations in Section V. The final section summarizes our main results.

II. NUMERICAL METHOD

The numerical technique we have employed is Smoothed Particle Hydrodynamic (SPH) method. In SPH, the fluid element is represented by discrete particles. This method is proven to be able to reasonably handle hydrodynamic phenomena in arbitrary geometric shape. More detailed description of SPH can be found from Monaghan (1992).

Although the code we are using is a fully three-dimensional one, we have confined the distribution of the particles in the disk so that we could achieve better resolution over the disk. The potential of the galaxy is assumed to be fixed in time because the time scale we are interested in is generally shorter than the time scale for potential changes. The potential generated by interstellar clouds can be negligible since the total amount stored in the clouds is very small. However, self-gravity of the disk sometimes could play important role under certain circumstances, and we have made a few simulations including the self-gravity of the gas. Self-gravity is particularly important where the gas concentration becomes significant. Such a concentration of gaseous material could cause dynamical instability (Shlosman 1999).

The cloud collisions are intrinsically highly supersonic because typical collisional velocity is order of several tens of km/sec while the internal sound speed is expected to be less than 1 km/sec. Thus the temperature at the shock front could be very high. In order to treat the collisions correctly, we need to solve the energy equation which is quite a difficult task. However, we simply assumed that the thermal temperature is always 10,000 K (Hernquist 1989). Such an *isothermal* assumption can be justified since the cooling time is much shorter than any other dynamical time scale we are interested in. Further, the temperature of 10,000 K is not actually the thermal temperature, but the temperature equivalent to the turbulent energy within interstellar clouds. Clearly, such a choice is somewhat arbitrary one, but the general behavior of the SPH particles is not very sensitive to the choice of the temperature.

We have used multi-grid method to compute the gravitational potential generated by the gas, although we have not considered the self-gravity in most cases.

III. MODEL GALAXIES

Surface photometry of spiral galaxies shows several distinctive components: central bulge, thin disk, and massive halo revealed only by the flat rotation curve. Barred galaxies have addition component of non-axisymmetric shape. The mass distribution of each component is difficult to trace, but the surface brightness distribution can be obtained by decomposition of observed profiles (Kormendy 1977; Ann & lee 1987). We then may determine the mass distribution of each component by assuming constant mass-to-light ratio for each component.

There is a growing evidence for the existence of central black hole in many galaxies (Kormendy & Richstone 1995). The mass of the black hole appears to be proportional to the mass of the 'hot component' of the galaxy: the bulge is a hot component of spirals while the entire galaxy is 'hot' for ellipticals (i.e., Magorrian et al.1998). Since we are more concerned on the large scale distribution of the gas, we ignored the central black hole in our simulations. The effect of the central black hole on gaseous disk should be negligible except for those very close to the black hole. However, the behavior of the gaseous material would be important in fueling the black hole.

We adopt simple analytic forms for the potential generated by each component. We describe the potential distribution of the model galaxies we have employed in the present study.

(a) Models for the Potential

The halo component, which gives rise to the flat rotation curve at outer radius, is assumed to have a logarithmic potential with finite core radius,

$$\Phi(r)_{halo} = \frac{1}{2} v_0^2 \ln(R_h^2 + r^2) + const, \qquad (1)$$

where R_h is the halo core radius, and v_0 is the constant rotation velocity at large r.

For the disk component, we adopt the Freeman's (1970) exponential disk which has of the following form for the potential;

$$\begin{aligned} \Phi(r)_{disk} &= \pi G \Sigma_0 r \left[I_0\left(\frac{r}{2R_d}\right) K_0\left(\frac{r}{2R_d}\right) \right. \\ &- \left. I_1\left(\frac{r}{2R_d}\right) K_1\left(\frac{r}{2R_d}\right) \right]. \end{aligned} \qquad (2)$$

Here R_d is the disk scale length, Σ_0 is the central surface density, and I_0, K_0, I_1, and K_1 are modified Bessel functions. The total disk mass is simply $M_{disk} = 2\pi\Sigma_0 R_d^2$.

As for the bulge component, we have assumed the Plummer's model to allow steep outward velocity increase from the GC;

$$\Phi(r)_{bulge} = -\frac{GM_{bulge}}{\sqrt{r^2 + R_b^2}}, \qquad (3)$$

where R_b is a parameter which controls the size of bulge. The bulges of real galaxies can be better represented by de Vaucouleurs' $R^{1/4}$-law, but we have taken Plummer model for simplicity.

The bar is a tri-axial component in three-dimension. However, our simulation is restricted to the two-dimensional disk. Thus we have adopted the following form of gravitational potential proposed by Long & Murali (1992) for the bar component,

$$\Phi(r)_{bar} = -\frac{GM_{bar}}{2a}\log\left(\frac{x-a+T_-}{x+a+T_+}\right), \qquad (4)$$

where $T_\pm = \sqrt{[(a\pm x)^2+y^2+b^2]}$, a and b are major and minor axis, respectively.

The properties (density, size and structure) of all potential generating components are assumed to be invariant in time.

(b) Model Parameters

The diversity of barred galaxies can be represented by a combination of different model parameters. Most components can be fully specified by the masses and sizes. The bar needs two more parameters: the axial ratio and pattern speed. In some models, we also introduced the inner nuclear bar which has been revealed by recent high resolution observations (Shaw et al.1995; Jungwiert, Combes, & Axon 1997; Regan & Mulchaey 1999). The parameters used in the present study are summarized in Tables 1, 2, and 3.

In all models, the simulation is performed for a disk of diameter 10 kpc. Thus, the mass of the halo refers to the mass within 10 kpc only. The total mass of the galaxy within 10 kpc is also fixed at $4\times10^{10}M_\odot$. By assuming $R_{CR}\approx 1.2\ a$ (Athanassoula 1992; Friedli 1999), the pattern speeds of the bars are chosen to fix the length of a bar as 6 kpc except for the model m35 of which the pattern speed is high enough to avoid ILRs. We have used the following units in expressing the mass, radius, pattern speed and time:

Mass: $4\times10^{10}M_\odot$

Lengths: 5 kpc

Time(τ_{bar}): 1.65×10^8 years

Angular Speed: 37.2 km/s/kpc

The symbols used in the table have the following meanings:

M_g: gas mass fraction

Ω_p pattern speed of the primary bar

D, B, B_a: mass fractions of disk, bulge, and bar.

M_{ib}: mass fraction of the inner nuclear bar.

a_s, b_s, Ω_s: parameters of the nuclear bar.

These models are broadly divided into three groups. The models of type A simulate the gaseous disks in early type barred galaxies, while the type B models represent the intermediate type($\sim$ SBa) galaxies. The type C models are intended for the analysis of the effects of dark halo, nuclear bar and self-gravity. The models for late type galaxies are also included in the type C models. All the models except for m34 and m25, which have no halo, assume that the dark halo has 10 % of the total visible mass within the diameter of 10 kpc. The models that take into account the self-gravity of the gaseous disks are designated by 's' at the end of model names given in the first column of the Tables 1-3.

Fig. 1 show the rotational velocities of the bulge, disk and halo components of the model galaxies as a function of radius. The rotational velocity due to the bar component is not shown because it is non-axisymmetric. In most cases, the contribution by the bar is not significant. Because we assumed a less massive halo except for the model C2, the rotation curves of the models dominated by bulge show the decline at large radius except for the model with rather extended bulge (e.g., A8). The flat rotation curves of most of the model galaxies are due to the disk component. This is evident from the rotation curve of C1 which has no halo component. The rising rotation curves of the models C5 and C6 are due to massive disks which are comparable to those of the late type spirals.

The angular frequencies corresponding to the rotational velocity generated by the axisymmetric components as a function of radius are given in Fig. 2. The pattern speeds of the bars are plotted as the horizontal dot-dashed lines in this figure. Most of the model galaxies have two ILRs inside the bar radius: the inner and outer ILR are designated by IILR and OILR, respectively. A highly concentrated bulge has very strong ILRs of which the IILR lies very near to the galaxy center. However, there are several models that have no ILR or only one ILR. As we will see in our results, the existence and locations of resonances play important role in driving the evolution of gaseous disk.

IV. RESULTS OF SIMULATIONS

We have started our simulations by distributing SPH particles uniformly over the disk on circular orbits. The bars are introduced slowly in a half of the bar's rotation period, and the simulations are carried out up to 10 rotations periods. However, we present the evolutionary sequence of models up to 5 rotations because there is little change in the distribution of SPH particles afterwards in most models. Due to the perturbations induced by the rotating bar, the SPH particles gain non-circular velocity components. The SPH particles then begin to interact hydrodynamically. Since we have made isothermal assumptions, the kinetic energy is efficiently dissipated after the hydrodynamic collisions.

(a) Evolution of Gaseous Disks

i) Type A models

Fig. 3 shows the evolution of gaseous disks of the models of type A. We have shown our results on rotating frame where the bar always lies horizontally. All the models in Fig. 3 have bulge masses comparable to or larger than disk masses. We fixed the axial ratio of

Table 1. Parameters for the Models of Type A

Model	M_g	R_h	R_d	R_b	a	b	Ω_p	D	B	B_a
A1	0.01	3.0	0.6	0.10	0.6	0.2	1.40	.29	.60	.10
A2	0.01	3.0	0.6	0.10	0.6	0.2	1.35	.26	.53	.20
A3	0.01	3.0	0.6	0.10	0.6	0.2	1.35	.44	.45	.10
A4	0.01	3.0	0.6	0.10	0.6	0.2	1.25	.39	.40	.20
A5	0.01	3.0	0.6	0.10	0.6	0.2	1.20	.34	.35	.30
A6	0.01	3.0	0.6	0.05	0.6	0.2	1.25	.39	.40	. 20
A7	0.01	3.0	0.6	0.15	0.6	0.2	1.25	.39	.40	.20
A8	0.01	3.0	0.6	0.20	0.6	0.2	1.25	.39	.40	.20
A9	0.01	3.0	0.3	0.10	0.6	0.2	1.50	.39	.40	.20
A10	0.01	3.0	1.2	0.10	0.6	0.2	1.15	.39	.40	.20

Table 2. Parameters for the Models of Type B

Model	M_g	R_h	R_d	R_b	a	b	Ω_p	D	B	B_a
B1	0.01	3.0	0.6	0.10	0.6	0.2	1.20	.59	.30	.10
B2	0.01	3.0	0.6	0.10	0.6	0.2	1.20	.52	.27	.20
B3	0.01	3.0	0.6	0.10	0.6	0.2	1.10	.46	.23	.30
B4	0.01	3.0	0.6	0.10	0.6	0.3	1.20	.52	.27	.20
B5	0.01	3.0	0.6	0.10	0.6	0.15	1.20	.52	.27	.20
B6	0.01	3.0	0.6	0.05	0.6	0.2	1.15	.52	.27	.20
B7	0.01	3.0	0.6	0.15	0.6	0.2	1.15	.52	.27	.20
B8	0.01	3.0	0.3	0.10	0.6	0.2	1.50	.52	.27	.20
B9	0.01	3.0	1.2	0.10	0.6	0.2	1.00	.52	.27	.20
B10	0.01	3.0	0.6	0.15	0.4	0.1	1.80	.52	.27	.20

Table 3. Parameters for the Models of Type C

Model	M_g	R_h	R_d	R_b	a	b	Ω_p	D	B	B_a	M_{ib}	a_s	b_s	Ω_s
C1	0.01	0.0	0.6	0.10	0.6	0.2	1.10	.52	.27	.20				
C2	0.01	1.0	0.6	0.10	0.6	0.2	1.40	.52	.27	.20				
C3^s	0.01	3.0	0.6	0.10	0.6	0.2	1.35	.26	.53	.20				
C4^s	0.05	3.0	0.6	0.10	0.6	0.2	1.20	.48	.27	.20				
C5^s	0.10	3.0	0.6	0.10	0.6	0.2	1.10	.72	.08	.10				
C6	0.10	3.0	0.6	0.10	0.6	0.2	1.10	.72	.08	.10				
C7^s	0.01	3.0	0.6	0.10	0.6	0.2	1.25	.39	.40	.19	0.01	0.06	0.02	6.20
C8	0.01	3.0	0.6	0.10	0.6	0.2	1.25	.39	.40	.19	0.01	0.06	0.02	6.20
C9	0.01	3.0	0.6	0.10	0.6	0.2	1.20	.52	.27	.19	0.01	0.06	0.02	1.20
C10	0.01	3.0	0.6	0.10	0.6	0.2	1.20	.52	.27	.19	0.01	0.06	0.02	6.00

^{s} Self-gravity model

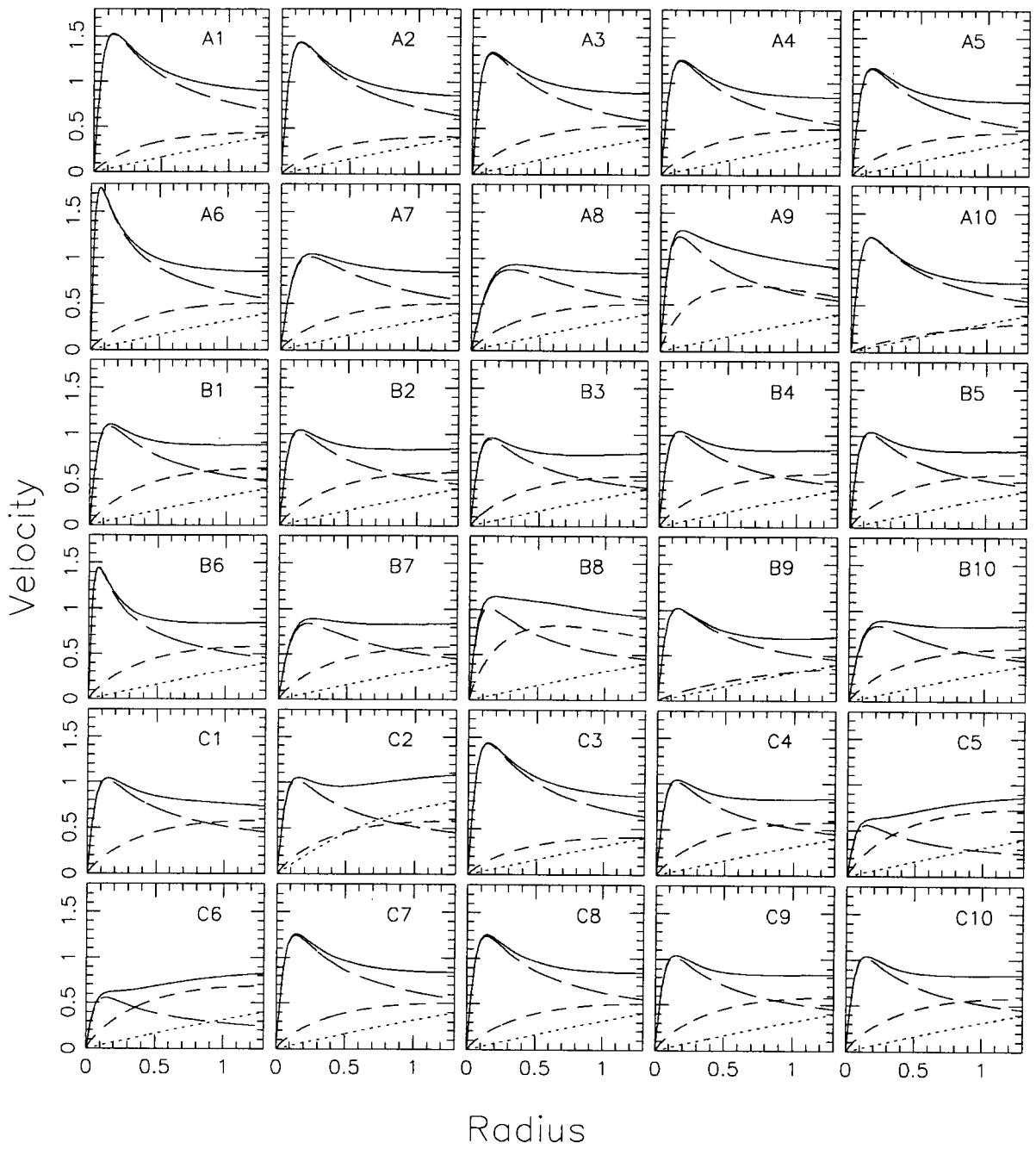

Fig. 1.— Rotation curves of model galaxies. The contribution from bar component is not included, because of non-axisymmetric nature. Since the halo comprises only a small amount of mass, most of the potential is generated by the bulge and disk. The contributions by the bulge, disk, and halo are represented by long dashed lines, short dashed lines, and dotted lines, respectively.

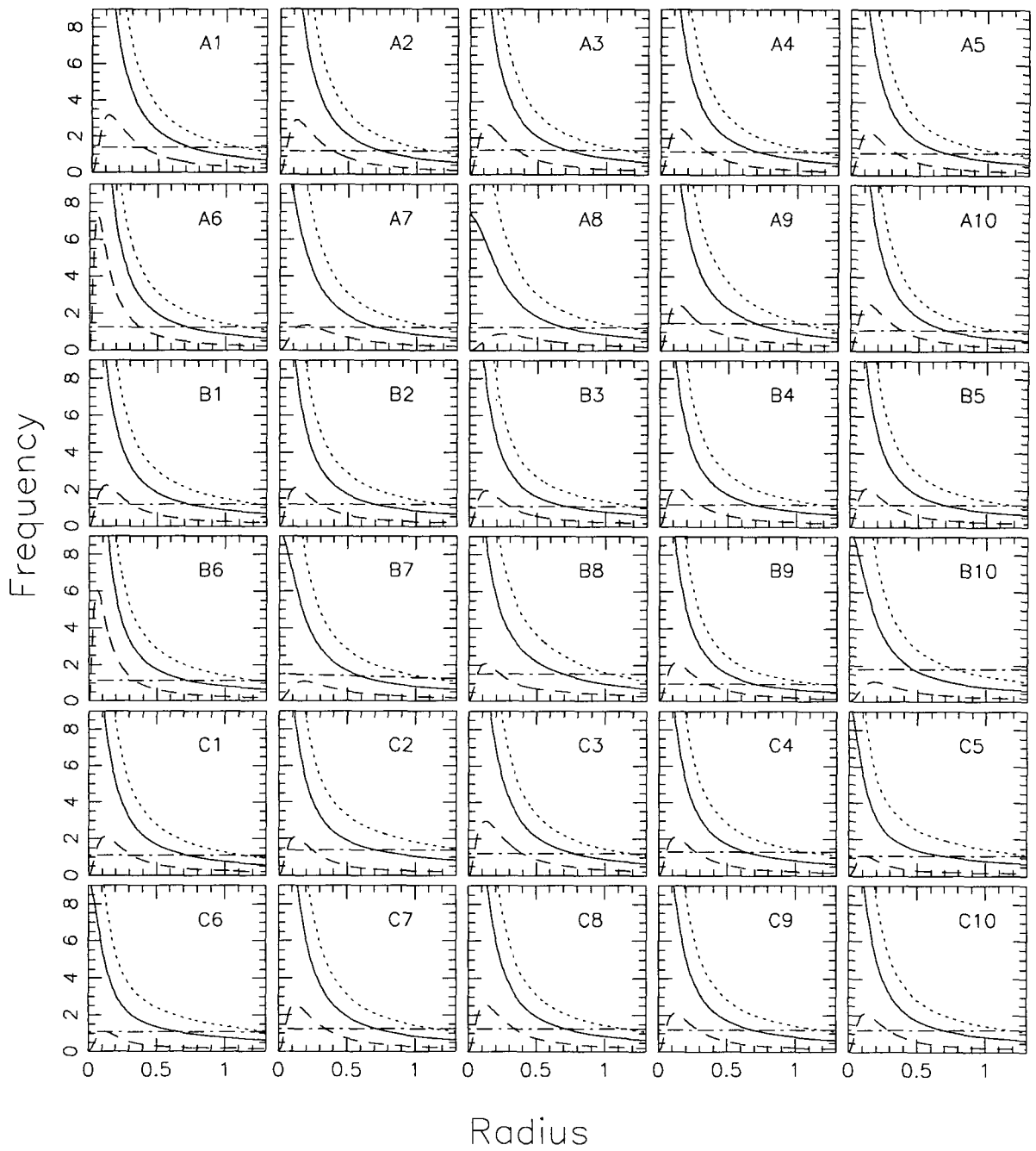

Fig. 2.— Angular frequencies corresponding to the rotation velocity shown in Fig. 1. Ω: solid, $\Omega+\kappa/2$: dotted, $\Omega-\kappa/2$: long dashed lines. Note the locations of resonances.

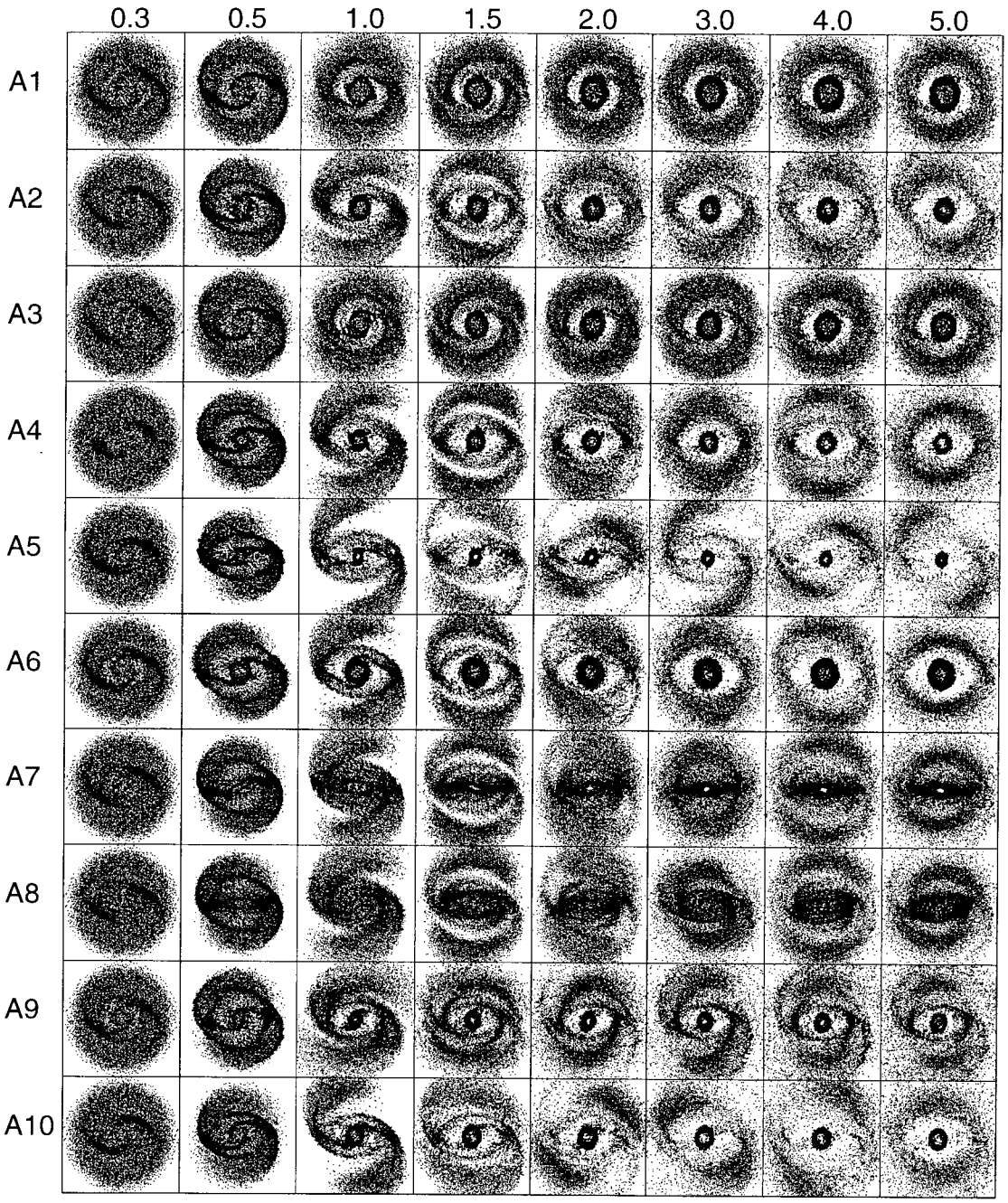

Fig. 3.— Evolution of gaseous disks for models A.

bar as $\frac{a}{b} = 3$. These models are suitable for the comparison with the early type barred galaxies. The general property of the evolution of the gaseous disk is the development of a global spiral pattern at earlier times and the formation of a nuclear ring near ILRs for the models with two ILRs. The models with no ILR, (e.g., A8) and with one ILR (e.g., A7) fail to develop nuclear rings. All the nuclear rings are aligned perpendicular to the bar which lies horizontally in the figures. Some models show the development of the outer ring which is very similar to the observed outer rings in barred galaxies.

The first two models (A1 and A2) have bulges whose masses are twice of the disks. The only difference between the models of A1 and A2 is the fractional mass of the bar: the bar of A1 is rather weak with the fractional mass of 0.1 while that of the model A2 is moderately strong with fractional mass of 0.2. The general morphology of the gaseous disk at the time of 5 rotations, which is characterized by two rings that resemble the nuclear ring and the outer ring of the observed barred galaxies, is quite similar to each other. Both of the nuclear rings are slightly elongated and they are aligned perpendicular to the primary bar.However, the early evolution of the two models are somewhat different. The spiral pattern of the gaseous disk of A1 is tightly wound from the early stage of evolution while that of A2 is somewhat open at $t \approx \tau_{bar}$ and evolves into more tightly wound shape similar to that of A1. The tightly wound spiral pattern of A1 evolves to the outer ring after two rotations. The sizes of the nuclear rings of the two models are also very different. Because the shapes of the rotation curves and the angular frequency distributions of the two models are very similar, the difference of the evolution is due to the bar strength caused by the different fractional mass of the bar.

The evolution of the second group of models (A3, A4 and A5) shows quite different morphology compared to those of the first group of models. This group is characterized by the comparable masses for the disk and bulge components with varying fractional masses of the bars, 0.1, 0.2, and 0.3, respectively. All the scale lengths of the three models are the same as those of the first two models. Among the models, the model A4 shows evolution of gaseous disk similar to that of the model A2. The model A3 shows the most tightly wound spiral pattern which evolves to a pseudo ring in later times while A5, which has the strongest bar, shows open spiral arms in the outer disk and a small compact nuclear ring near IILR.

The third group of models (A6, A7, and A8) represents galaxies with different degrees of central mass concentration. As shown Fig. 2, a highly concentrated model gives strong ILRs while less concentrated model gives a weak ILR or no ILR. The evolution of the gaseous disk appears to depend on the existence of ILRs. The most centrally concentrated mass model A6 shows large perpendicular nuclear ring while the least concentrated mass model A8 shows no nuclear ring. The lack of nuclear ring is due to the lack of ILR in model A8. In the less centrally concentrated model A7, SPH particles inside the bar radius become distributed along the bar.

The last two models (A9 and A10) show well developed nuclear rings with moderate size. These models also have comparable masses of the bulge and the disk but their disk scale lengths are different from those of the other models which have comparable masses of the bulge and the disk. The model A10 that has a large disk scale length shows a strong density enhancement along the bar which resemble leading dust lanes in real barred galaxies. The strength of this feature is reduced gradually but remain visible until 5 rotations. The short disk model of A9 shows multiple spiral arms, inner ring, and nuclear ring. The outer spiral arms remain open up to 5 rotations. The inner ring of A9 is quite elongated and aligned parallel to the bar. All the models in Fig. 3 have the inner rings at earlier times but most of them are transient features.

ii) Type B models

Fig. 4 shows the evolution of the gaseous disks exposed to bar forcing. The models in this group are constructed to simulate the evolution of gaseous disks of intermediate type barred galaxies. The typical Hubble type relevant to this group of models is SBb. We keep the bulge-to-disk mass ratios at 0.5 for all the models and the fractional mass of bar at 0.2 except for the two models B1 and B3. They are included to investigate the effect of bar mass fractions. We varied the scale lengths of the bulge and disk as well as the length and axial ratio of the bar. The evolution of the general morphology of the gaseous disks shows significant differences among models. Most of the models show nuclear rings but the morphology of the nuclear rings are very different. All the models show open outer spiral arms at one bar rotation but some of them evolve to the outer rings or pseudo rings in 5 rotations.

The first group of models (B1, B2, and B3) are intended to study the effect of the bar mass fractions on the evolution of the gaseous disks. The first model B1 has the smallest bar fraction of 0.1 and the third model m11 has the largest bar mass fraction of 0.3. The general morphology of gaseous disk of B1 is very different from that of the other two models B2 and B3. The model B1 shows a well developed nuclear ring which is aligned perpendicular to the bar while the nuclear rings of the models B2 and B3 are aligned parallel to the bar. The size of the nuclear ring of B1 is about three times larger than that of the nuclear bars of B2 and B3. There are straight dust lanes in B3 which has the strongest bar. The outer spiral arms of B1 evolve to the outer ring in a very short time.

The second group of models (B4 and B5) have the same model parameters as those of B2, which is the central model of the type B, except for the bar axial ratio. The evolution of B4 is similar to that of B1,

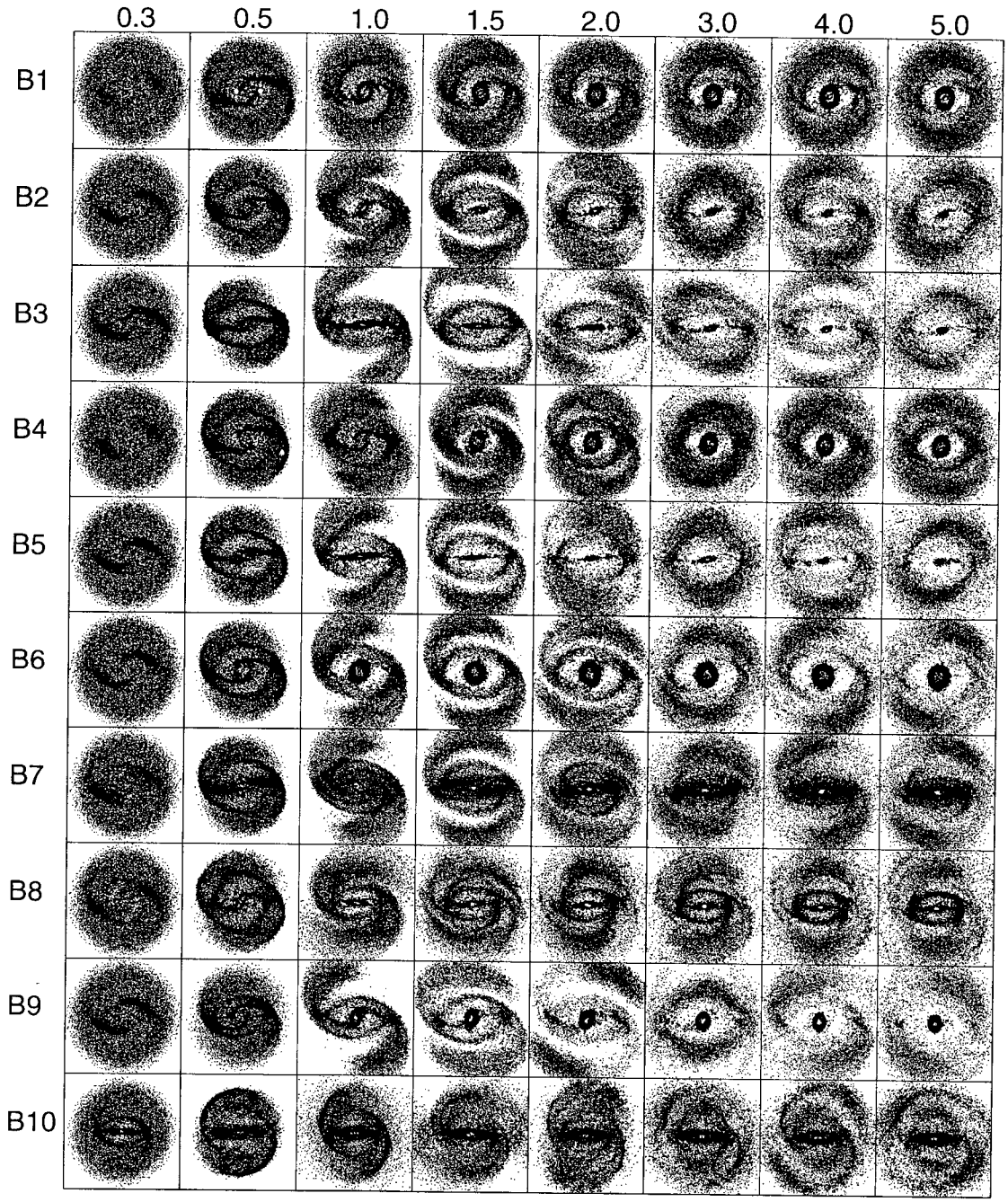

Fig. 4.— Evolution of gaseous disks for models B.

which is characterized by a well developed nuclear ring and outer spiral arms which evolve to an outer ring. The reason for the similarity of the two models B4 and B1 is the similar bar strength. The model B5 which has a large axial ratio of 4 shows evolution similar to that of the model B3. The reason for the similarity of these two models are the same as that for B4 and B1. The model B5 has a strong bar due to the large axial ratio of the bar while the model B3 has a similarly strong bar due to the large mass fraction of the bar. Thus, the evolution of the gaseous disks is strongly dependent on the strength of the bars.

The third group of models (B6 and B7) reveals the contrast between the morphology of the gaseous disks with different central mass concentration. As shown in Fig. 1 and 2, the model B6 has a highly concentrated bulge model that allows the strong ILRs while the model B7 has a weakly concentrated bulge model that leads to no ILR. The early evolution of B6 resembles those of A6 and B4. The former one has the same model parameters as that of B6 except for the bulge-to-disk ratio. The latter one has a weak bar due to its small axial ratio. This means that the effect of reducing the strength of bar is similar to that of increasing the degree of central mass concentration. The evolution of the gaseous disk of B7 shows an intermediate morphology between A7 and A8. The model A7 has one ILR while A8 has no ILR like B7.

The fourth group of models (B8 and B9) shows the gaseous disks of the model galaxies which has small and large disk scale lengths, respectively. These models have the same parameters as those of the models A8 and A10 except for the bulge-to-disk ratio. The morphology of the outer spiral arms and the inner ring of B8 is similar to that of A9 but the nuclear ring of B8 is highly elongated along the bar and is connected to the straight dust lanes in the center of the bar axis. The inner ring structure observed in A7 is also seen in B8 with much higher density. The extended disk model of B9 shows a well developed perpendicular nuclear ring with highly curved dust lanes similar to those of A10.

The last model (B10) is designed to see the effect of a high pattern speed which does not allow the ILR. The length of the bar is reduced to 2 kpc to match the constraint of $R_{CR} \approx 1.2a$. However, we take the the bar axial ratio as 4 to have a strong bar. We also reduced the central mass concentration to allow that the relative strength of the non-axisymmetric force is high enough to drive strong gravitational torque in the central region. As expected from no ILR condition, there is no nuclear ring but a large fraction of the SPH particles lie along the bar, which are similar to other models that have no ILR. The outer spiral arms that evolve to the outer pseudo ring are much narrower than others. However, the most pronounced feature is the well defined inner ring that survives until the end of the simulation. This inner ring is a little bit elongated in the direction perpendicular to the bar. There is no other model which has an inner ring aligned perpendicular to the bar.

iii) Type C models

Fig. 5 shows the evolution of the gaseous disks in various environments, such as galaxies having massive disk, massive halo or nuclear bar. We include the self-gravity of gaseous disk in some models of this group. The models with negligible bulges are suitable for the comparison with the late type spirals. We include the nuclear bars because a large fraction of barred galaxies have nuclear bars (Shaw et al.1995) and they are thought to be effective for fueling the AGNs (Shlosman, Frank, & Begelman 1989). As shown in Fig. 5, the self-gravity of gas affects the evolution of gaseous disk significantly in the models with high gas fractions while it is not important if the gas comprises less than 5 % of the total mass. However, the self-gravity of gas can induce the infall of gas to the nucleus even in the models with negligible gas fractions. The global morphology of the gaseous disks is not affected by the inclusion of nuclear bars, but it drives the mass inflow to the nucleus itself. We considered the synchronous and fast nuclear bars together to see the effect of the pattern speed of the nuclear bar.

The first two models (C1 and C2) are introduced to investigate the effect of dark halo. The evolution of the general morphology of the no halo model (C1) is very similar to that of the model of large disk scale length (B9) except for the evolution of the dust lanes, while the evolution of the model with massive halo resembles that of the model with small disk scale length (B8). The similarities of these models result from the similar density gradient in the central region because the massive halo model has compact core ($R_h = 1$) which provides a steep density gradient near the galactic center while no halo model gives a shallow density gradient. The steep density gradient provided by the small halo core radius have similar effects on the evolution of the gaseous disk with the density gradient provided by the short disk model. However, the detailed morphology of the massive halo model (C2) is somewhat different from that of the short disk model due to the different origin of the steep density gradients of the two models. The outer spiral arms of C2 become the outer pseudo ring at 5 rotations while the outer spiral arms of B8 remains as open spiral arms.

The second group of models (C3, C4, C5, and C6) reveals the effect of the self-gravity of gas. The models with small gas mass fraction (C3 and C4) seem to be little affected by the self-gravity because the morphology is virtually identical to the similar models without the self-gravity. The only visible effect of the self-gravity in these models is the infall of gas into the nucleus of C4 which has gas mass fraction of 5 % of the total visible mass. The models with 10 % gas (C5 and C6) show, however, very different evolution due to self-gravity. The self-gravity model (C5) shows pronounced multiple spiral arms in the disk while the model without the self-

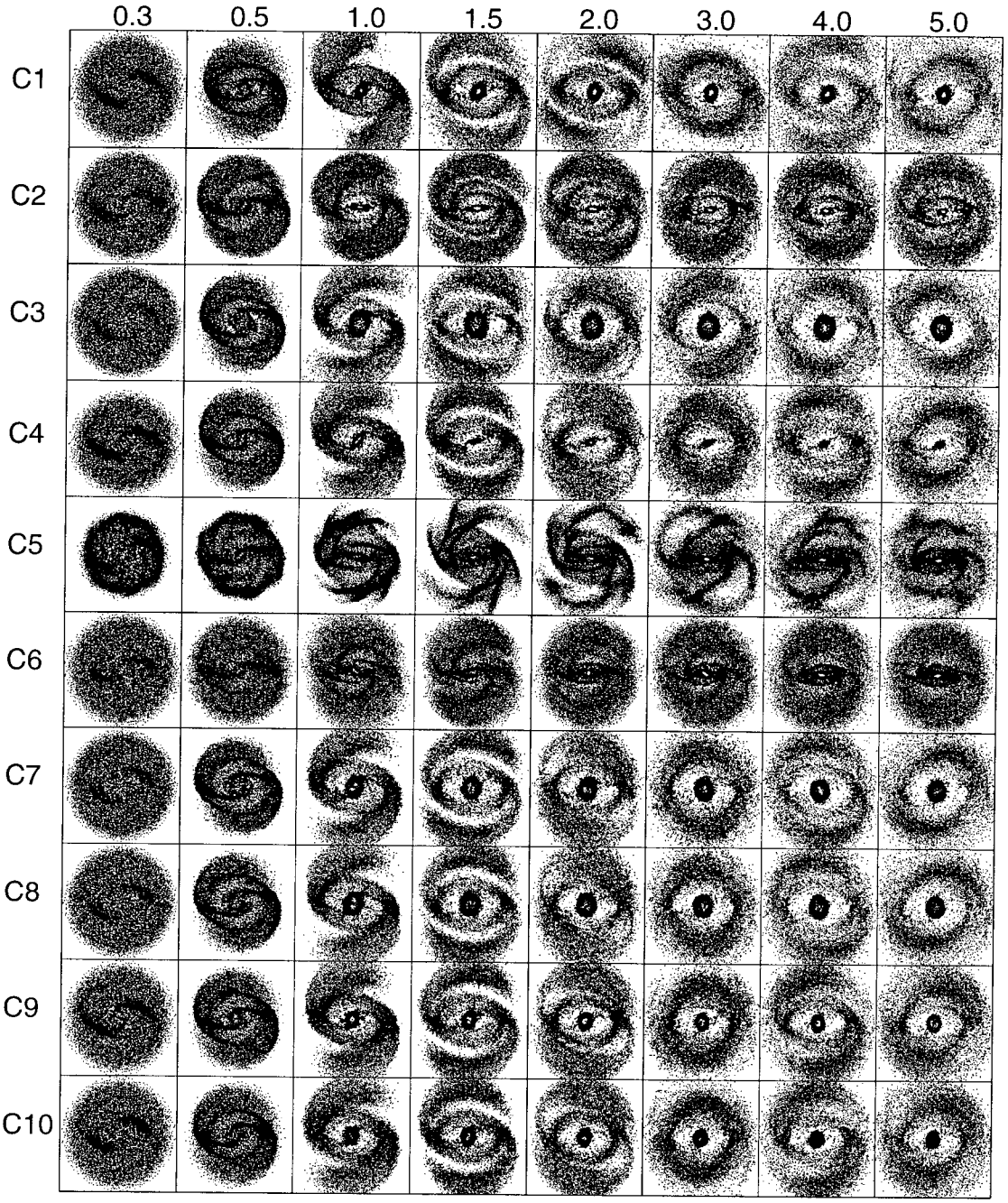

Fig. 5.— Evolution of gaseous disks for models C.

gravity (C6) shows rather simple evolution. The third group of models (C7, C8, C9, and C10) is characterized by the nuclear bars. In general, the global morphology of the gaseous disk is not affected by the inclusion of the nuclear bar. The nuclear bar, however, affects the nuclear morphology by driving mass inflow toward the nucleus within the ILRs. Because there is no difference between the morphology of the two models, one with the self-gravity (C7) and the other without (C8), the effect of self-gravity is negligibly small in these models, compared to the effect of the nuclear bar itself. Thus, the broader nuclear rings of C7 and C8, compared with those of m1 which is the standard model of comparable masses for the bulge and the disk, are due to the effective mass inflow driven by the nuclear bars that rotate faster than the primary bars.

In case of the small bulge models (C9 and C10), the inclusion of nuclear bars affects the nuclear morphology so much that the size and the orientation of the nuclear rings of these models are quite different from that of the standard model of this type (B2). The nuclear ring of B2 is smaller than those of C9 and C10. It is aligned nearly parallel to the bar while the nuclear rings of C9 and C10 are aligned perpendicular to the bar. The small difference of the nuclear morphology of the two models, C9 and C10, is due to the different pattern speed of the nuclear ring. We assumed the synchronous rotation for C9 and five times faster rotation for C10, respectively. As is evident from Fig. 5, a fast nuclear bar drives more inflow of gas to the nucleus than the synchronous nuclear bar. The reason for the effective mass inflow for the fast nuclear bar is that the fast nuclear ring perturbes the orbits of SPH particles near the ILRs more frequently than the synchronous one.

(b) Velocity Field

Fig. 6, 7, and 8 show the snap shots of the velocity fields of selected models listed in Tables 1, 2, and 3, respectively. We present three snap shots for each model to show how the interesting features such as rings and spiral arms evolve. The numbers in the top of the diagrams represent the time in units of the bar's rotation period. The size of each diagram is 11 kpc in one dimension. We plotted the velocity of randomly selected 3000 particles to achieve better resolution. The arrows represent the velocity vector of SPH particles relative to the bar. Because the bar lies horizontally in the frame corotating with the bar that rotates counter-clockwise, the clockwise motion represents the trailing gas while the counter-clockwise motion indicates the leading gas. The SPH particles outside the corotation radius R_{CR}, which is seen as the locations of the zero velocity particles, trail the bar and the SPH particles inside the R_{CR} lead the bar.

Th velocity field in Fig. 6-8 provides intuitive understanding of the gas flow which leads to the formation of rings and dust lanes. The outer rings are believed to be associated with the outer Lindblad resonance (OLR) and the inner rings and the nuclear rings are related to the ultra harmonic resonance (UHR) and the inner Lindblad resonance (ILR), respectively (Freeman 1996; Combes 1996). Fig. 6 shows clearly the evolution of the trailing spiral arms which consist of SPH particles that move outward outside the R_{CR}. The outward motion is caused by the acquisition of the angular momentum from the bar. The trailing spiral arms tend to evolve to the outer rings and outer pseudo rings. Fig. 6 shows many examples of the evolution of the trailing spiral arms to the outer rings. A typical example is the m1 model. In the majority of the models, the outer rings rotate slowly relative to the bar. However, the pseudo rings rotate quite rapidly (A3, B7 and B10).

The inner rings are more easily identified in the velocity field diagram due to the pronounced leading motion of the SPH particles that constitute the inner rings. One exception is the inner ring of B10 which is not apparent in the velocity field diagram while it is well identified in the particle distribution diagram of Fig. 5. Typical examples which show pronounced leading motions are the inner rings of A6 and B4. The former is an example of circular inner ring and the latter is that of the highly elongated one. The orbits of the SPH particles in the inner rings are x1 family of orbits which are elongated along the bar. The inner rings maintained by the x1 orbits can remain for several rotation periods. But they become more circular in the models with strong ILRs. Most of the inner rings disappear after several rotations by losing the gas gradually due to the gravitational torque of the bar.

There are a few inner rings which are highly elongated along the bar. The orbits of these inner rings also show large leading motion and survive up to the end of the simulations. All of these highly elongated inner rings are observed in the models with somewhat weak ILRs (A9, B8, and C2). The nuclear rings associated with these inner rings are small compared to other models. Both A9 and B8 have disks with small scale length although the bulge-to-disk ratio of A9 is twice of B8. The similarity of the shape and orbital property of the inner rings of these models are due to the similar density gradient of these models. The compact core of C2 plays similar role with the short disks of A9 and B8. However, the orbits of the nuclear rings of the three models are different due to the different contribution of the non-axisymmetric force in the central region.

The orbital properties of the SPH particles in the models of one ILR (A7, C5, and C6) or no ILR (A8, B7, and B10) are significantly different from the other models. In these models, the SPH particles can travel close to the nucleus because there is no strong obstacle which prevents the SPH particles from approaching the nucleus. Majority of the particles move on the x1 orbits which are the main family of orbits that constitute the bars. Due to the dominance of the x1 orbits, there is no nuclear ring in these models. However, despite the similar orbital properties of these models, the mor-

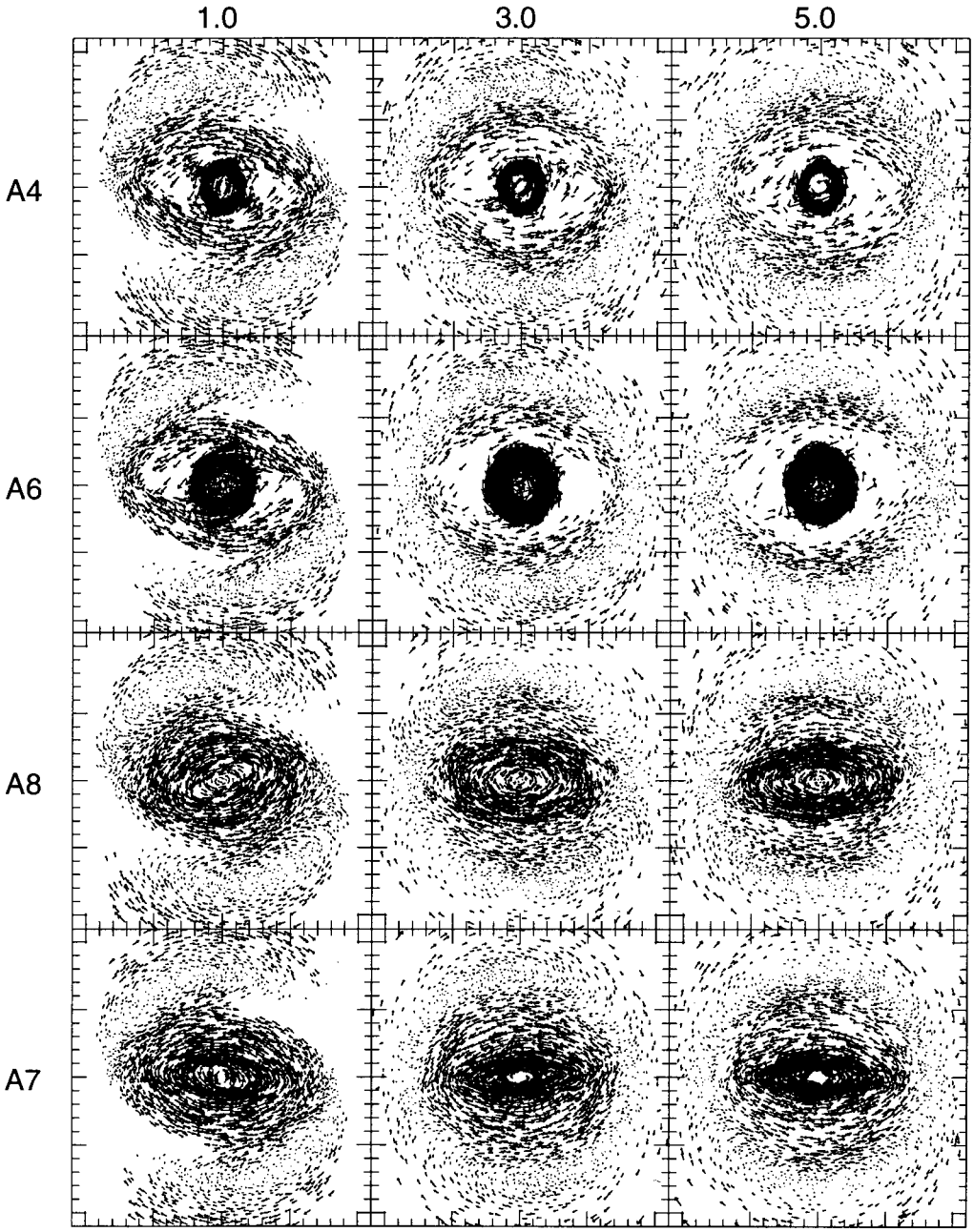

Fig. 6.— Snap shots of the gas velocity of the selected models of type A

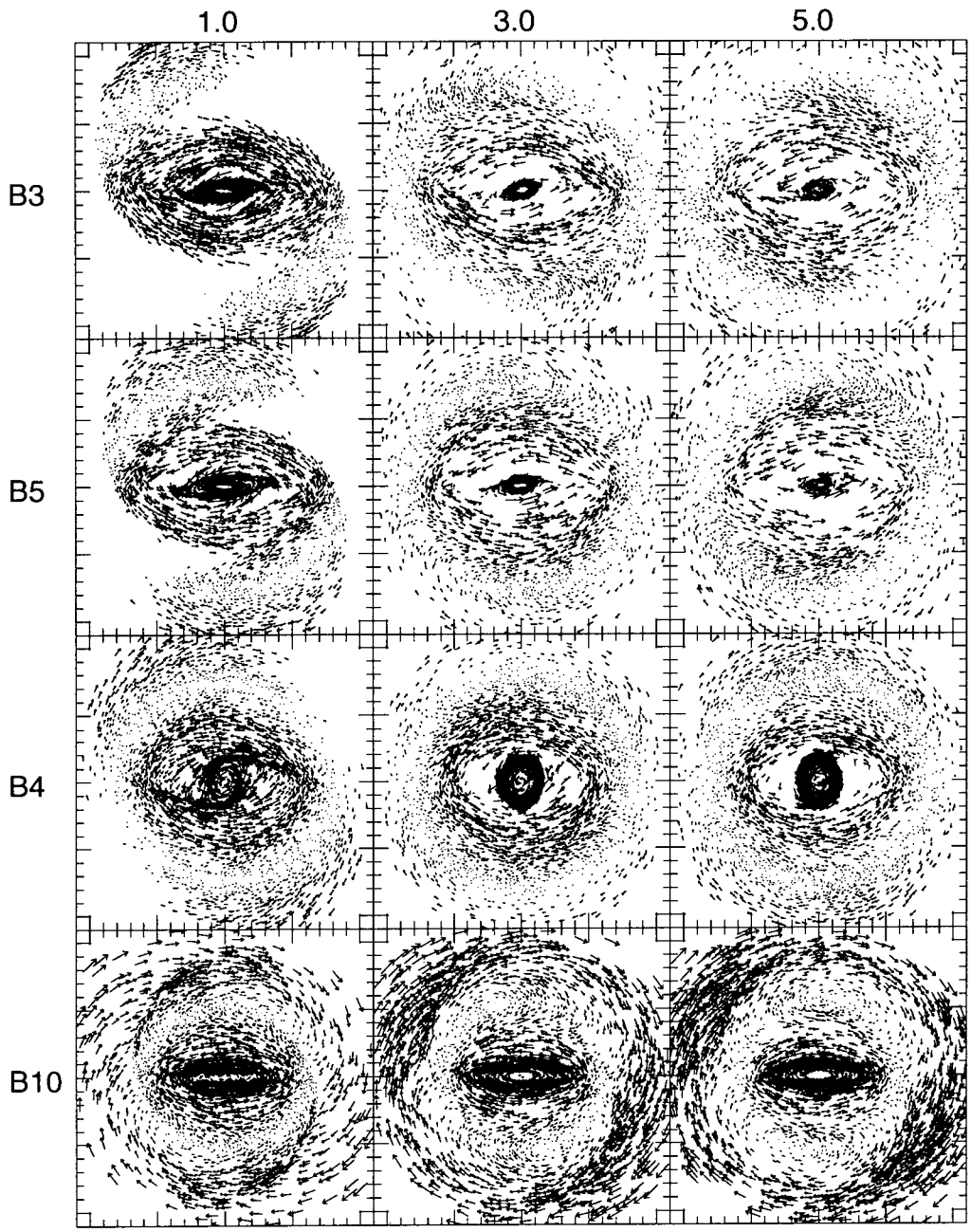

Fig. 6.— Snap shots of the gas velocity of the selected models of type B.

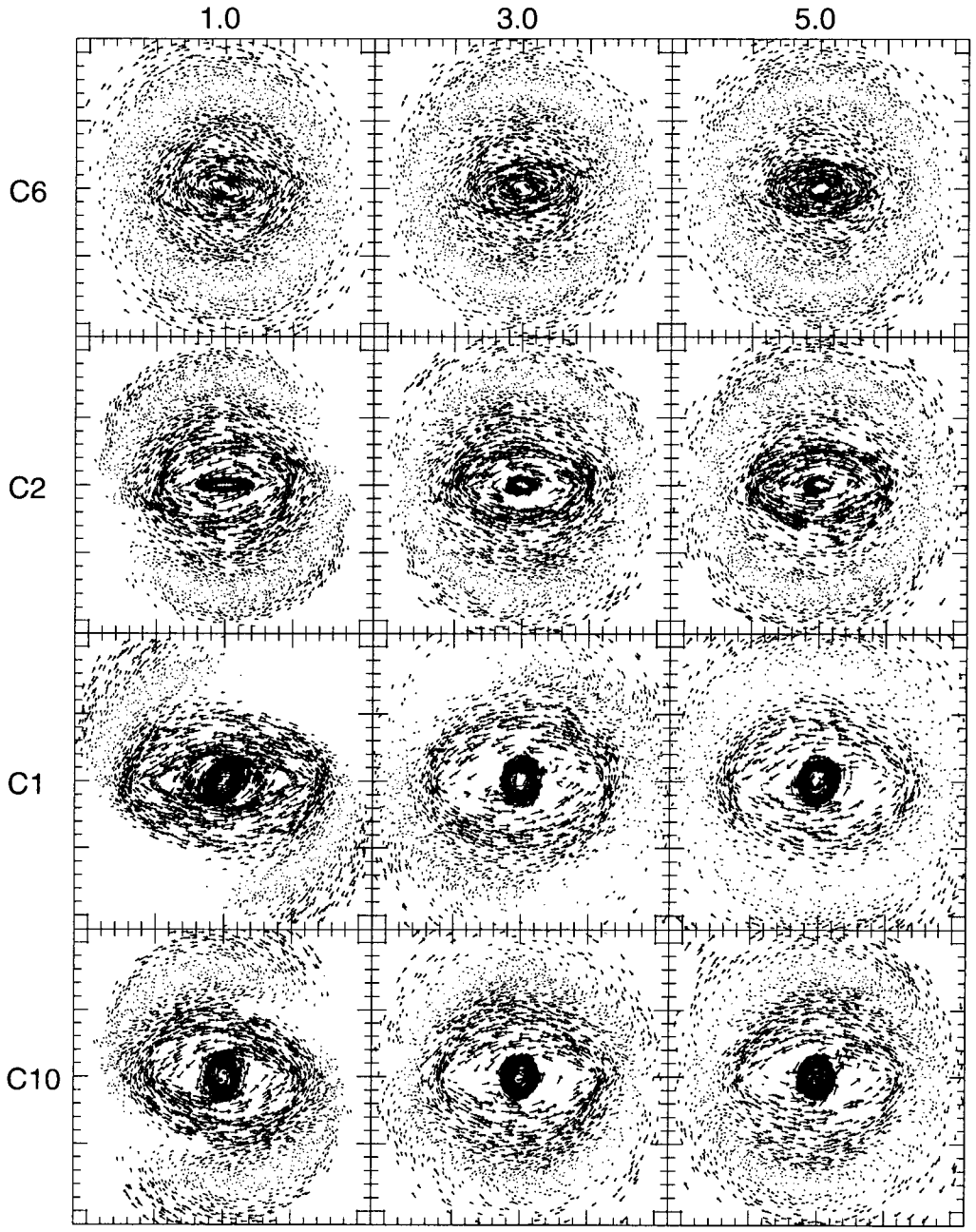

Fig. 6.— Snap shots of the gas velocity of the selected models of type C.

phologies and velocity fields of these models are quite different due to the different cause of the absence of the strong ILRs. Among these models, the comparable mass model of A8 shows most pronounced difference from the others in the particle distribution and orbital shapes. In the A8 model, the SPH particles are populated nearly uniformly in the bar region, including the nucleus itself, except for the shocked regions of spiral pattern which are indicated by the abrupt changes of the velocities in the earlier phase. The shape of the ensemble of the orbits looks like bar itself. In all the other models, there is no SPH particles which fall into the nucleus itself even though they can reach very close to the nucleus. Rather, the orbits of the other models are heavily crowded and they induce strong shocks in the leading edges of the bar. The reason for the difference between the orbital characteristics of the individual models is the different relative strength of the non-axisymmetric force in the central region.

It is well known that the existence of at least one ILR is necessary for the formation of the nuclear ring (Combes 1996). However, as described above, nuclear rings hardly form in the absence of strong ILRs. Most of the well developed nuclear rings are associated with the strong ILRs. Strong ILRs perturb the particles in the x1 orbits into the x2 orbits which are the main orbits of the nuclear ring. This is the reason for the orientation of the nuclear rings perpendicular to the bar. As shown in Fig. 6, most of the nuclear rings are associated with strong shock fronts, at least in earlier times. The shock fronts are easily identified by the abrupt changes of the particle velocities. The dust lanes in barred galaxies are believed to be the shock fronts (Athanassoula 1992). In Fig. 6-8, we see that most of the shock fronts inside the bar radius are located in the leading edges of the bar. The nuclear rings grow until there is no gas inflow from the disk. In most cases, the inflow of gas ceases after several rotations.

The nuclear rings formed in the strong bar potentials tend to be elongated parallel to the bar unless the central bulge is massive enough. Examples of such nuclear rings can be seen from B3 and B5. As shown in Table 2, the strong bars of these models are due to the large bar mass fraction (B3) and the large bar axial ratio (B5), respectively. In these models, the nuclear rings form in a highly elongated shape from the highly shocked gas. The size of the elongated rings decrease with time by the shrinking of the rings. Such a shrinking of the nuclear ring is implied in the nuclear ring of NGC 4314 (Combes et al.1992) which has a very strong bar (Benedict et al.1992; Ann 1999).

(c) Observational Implications

The numerical simulations are done only for gaseous material, but galaxies are most extensively studied with optical images that traces mostly the distribution of stars. Therefore, direct comparison between optical images and the simulated results cannot be done. The distribution of the gas can be studied by the molecular line observations with radio telescope. Unfortunately, radio telescopes have rather poor resolution compared to optical telescopes. There are several millimeter arrays which have resolution of order of arc seconds. In principle, high resolution observations with molecular lines would give a direct information on the gas distribution, but the strength of the emission lines also depends on the abundance of specific molecules chosen for the study. It would be still desirable to conduct a mapping of selected gas-rich barred galaxies with millimeter arrays.

The concentration of gas would induce star formation activities. Thus sensitive observations of barred galaxies with H_α filter should also provide the information regarding the gas in the galaxies.

The galactic potential is affected by the distribution of the gas. Since the contribution by the gas is expected to be small, the resulting concentration of stars in the region where the gas is concentrated should not be a significant effect. However, it would be interesting to obtain a 'residual' map after subtracting the axisymmetric, smooth components from the optical images of barred galaxies.

V. SUMMARY AND CONCLUSIONS

We have performed SPH simulations of the gaseous disks of barred galaxies. Most of the model galaxies have rather strong bars but we also studied some models with rather weak bars. The evolution of the gaseous disks of barred spiral galaxies depends on the relative strength of non-axisymmetric force. There are several ways to define the strength of bars: we defined the bar strength by the fractional mass, the axial ratio, and the pattern speed of the bar. The last parameter determines the length of the bar by assuming that the bar ends near the corotation. However, the relative strength of the non-axisymmetric force is determined by not only the bar strength but the mass models of the bulge and disk which can be defined by the fractional mass and the scale lengths of these components. From the extensive SPH simulations, we draw following conclusions:

1. The evolution of morphology of the gaseous disk depends on the relative strength of non-axisymmetric force to the symmetric one. When there exist two ILRs, it is difficult to avoid the gas inflow that forms the nuclear rings. In most cases, the nuclear rings align perpendicular to the bar. The aligned nuclear rings can be formed only in the models with extremely strong bars and they shrink across the ILRs.

2. The most critical parameter that determines the nuclear morphology of gaseous disk is the central mass concentration which is mainly determined by the bulge scale length. There is virtually no way to avoid the ILRs in the models of centrally concentrated bulges.

3. The evolution of the gaseous disk is not much

affected by the self-gravity when the gas mass is a negligible compared to the total mass (i.e., less than 5 %). But the self-gravity is crucial for the dynamics of the nuclear region by driving the inflow of gas toward the nucleus.

4. The nuclear bar does not affect the evolution of the gaseous disk except for the evolution of the nuclear region where it drives inflow of gas to the nucleus. The fast rotating nuclear bar is more effective than the synchronous bar to drive the gas inflow.

5. The inner rings are developed from the spiral pattern near corotation. Most inner rings are transient features unless there is a steep density gradient due to either a small disk scale length or small halo core radius. The spiral arms in large bulge models tend to evolve to the outer rings or pseudo rings.

Most of the calculations were conducted by the High Performance Supercomputing Laboratory of PNU. We thank Dr. H. Kang for many useful comments and helps in carrying out our numerical simulations. This research was supported by Korea Research Foundation non-directed research grant No. 1997-001-D00163.

REFERENCES

Ann, H. B., 1999, JKAS, 32, 83

Ann, H. B., & Lee, S-W. 1987, JKAS, 20, 49

Athanassoula, E. 1992, MNRAS, 259, 345

Benedict, G, F., Higdon, J. L., Tollestrup, E. V., Hahn, J., & Harvey, P. M. 1992, AJ, 103, 757

Binney, J., Gerhard, O.E., Stark, A.A., Bally, J., & Uchida K.I. 1991, MNRAS, 252, 210

Combes, F. & Gerin, M., Nakai, N., Kawabe, R., & Shaw, M. A. 1992, A&A, 259, L27

Contopoulos, G., & Mertzanides, C. 1977, A&A, 61, 477

Contopoulos, G. 1981, A&A, 102, 265

Freeman, K. C. 1996, ASP Conference Series, 91, 1

Friedli, D. 1999, ASP Conference Series, 187, 88

Hernquist, L. E. 1989, Nature, 340, 687

Jungwiert, B., Combes, F, Axon, D. J. 1997, A&AS, 125, 479

Kormendy, J. 1977, ApJ, 217, 406

Kormendy, J., & Richstone, D. 1995, ARA&A, 33, 581

Lee, C. W., Lee, H. M., Ann, H. B., & Kwon, K. H., 1999, ApJ, 513, 242

Long, K., and Murali, C. 1992, ApJ, 397, 44

Magorrian, J., Tremaine, S., Richstone, D., Bender, A, Faber, S. M., Gebhardt, K., Green, R., Grillmair. C., & Kormendy, J. 1998, AJ, 115, 228

Monaghan, J. J. 1992, ARA&A, 30, 543

Regan, M. W., & Mulchaey, J. 1999, AJ, 117, 267

Shaw, M., Axon, D., Probst, R., & Gatley, I., 1995, MNRAS, 274, 369.

Shlosman, I. 1999, ASP Conference Series, 187, 100